PIER Letters

(Received 3 January 2024, Accepted 23 February 2024, Scheduled 29 February 2024)

Millimeter-Wave Dual-Frequency Dual-Polarized Circular Airy OAM Beams by Tensor Holographic Impedance Metasurface

Hui-Fen Huang* and Ying-Jing Ma

School of Electronic and Information Engineering, South China University of Technology, Guangzhou 510641, China

ABSTRACT: In this paper, analytical formulas for tensor holographic impedance metasurface (THIMS) are presented to generate circularly polarized (CP) circular Airy orbital angular momentum (OAM) multibeams with flexibly independent control of the beam direction, polarization, and OAM mode. As an example, a millimeter-wave THIMS is designed to generate CP circular Airy OAM dual beams: Beam-I: ($\theta_1 = 0, \varphi_1 = 0$, LHCP, $l = +1$, 36 GHz), Beam-II: ($\theta_2 = 0, \varphi_2 = 0$, RHCP, $l = 0$, 30 GHz). To the knowledge of the authors, there is very little literature on circular Airy beams that have been generated with THIMS. Compared with the published metasurface on Airy beam, the created THIMS has the following advantages simultaneously: dual frequencies, dual CP, small size $30\lambda_0$ at 30 GHz, high conversion efficiency (CE) (above 40%), long nondiffractive distance (ND) (up to $134.4\lambda_0$), high OAM purity (above 89%), co-modulation for polarization, beam direction and OAM mode. The generated circular Airy OAM beams can be used in near-field scenarios such as high-efficiency wireless power transmission (WPT), high-capacity communication systems, and high-resolution imaging.

1. INTRODUCTION

In 2010, circular Airy beams with radial symmetric structure were reported, which has non-diffraction and abrupt auto-focusing characteristics [1]. A beam abruptly focuses its energy right before a target while maintaining a low-intensity profile until focusing. It is crucial for many applications, such as medical treatment [2] and the generation of a light bullet [3]. The Airy beam that carries OAM has non-diffraction and sudden self-focusing properties, as well as infinite dimensions, which have great application potential in high data rates and high-capacity communication systems. An Airy beam multifunctional terahertz metasurface is proposed for multiple functions under different polarization waves [4]. A 2-D Airy beam with self-bending and non-diffraction characteristics is generated and verified at microwave frequencies by using a metasurface composed of a single-layer of strip resonator [5]. However, it is difficult to obtain circular Airy multibeams with flexible co-modulation of polarization, beam direction and OAM mode by conventional technique. THIMS is a good solution, can simultaneously control frequency, polarization, and OAM mode, and has high aperture efficiency (AE) [6]. In addition, it is convenient to realize arbitrary polarization by THIMS. Therefore, THIMSs have attracted considerable attention recently [7–10]. However, to the knowledge of the authors, there is no work on Airy beam generated by the THIMS.

In this paper, analytical formulas are presented for CP circular Airy OAM multibeams with flexible co-modulation of SAM, OAM mode, and beam direction. As an example, a millimeter-wave THIMS is designed for dual-frequency dual CP circular Airy OAM beams. Compared with the published metasurface on Airy beam, the created THIMS has the following advantages: dual frequencies, dual CP, small size $30\lambda_0$ at 30 GHz, high CE (above 40%), long ND (up to $134.4\lambda_0$), high OAM purity (above 89%), co-modulation for polarization, beam direction, and OAM mode.

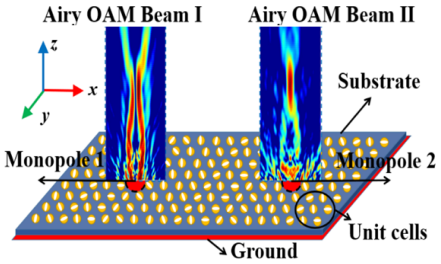

FIGURE 1. Schematic of the THIMS for circular Airy OAM beams.

2. DESIGN PRINCIPLE

The schematic of the THIMS for CP circular Airy OAM beams is shown in Fig. 1. The THIMS is located in the xoy plane, and the origin of the coordinate system is at the center. The THIMS controls the electromagnetic wave by adjusting the surface impedance distribution in the THIMS. The surface impedance distribution calculation is described as follows. To generate an objective wave, the value of the holographic modulated impedance $\overline{\overline{Z}}$ required at each position $(x, y, 0)$ on the THIMS can be derived from the interference between the mth objective wave and the excitation surface current $\vec{J}_{surfm}$ [11]:

$$\overline{\overline{Z}} = \begin{pmatrix} Z_{xxm} & Z_{yxm} \\ Z_{xym} & Z_{yym} \end{pmatrix} = jX_m\overline{\overline{I}} + j\frac{M_m}{2\sum_{m=1}^{N}}\sum_{m=1}^{N}\left\{\vec{E}_{radm}\otimes\vec{J}^{+}_{surfm} - \vec{J}_{surfm}\otimes\vec{E}^{+}_{radm}\right\} \quad (1)$$

* Corresponding author: Hui-Fen Huang (huanghf@scut.edu.cn).

where Z_{xxm} and Z_{yym} are tensor impedance components for co-polarization, and Z_{xym} and Z_{yxm} are tensor impedance components for cross-polarization. $\overline{I}$ is a 2×2 identity matrix. N, $+$, and $\otimes$ are the number of object wave beams, the Hermitian conjugate, and the Kronecker product, respectively. Here, X_m and M_m are the average reactance and modulation index of the surface impedance, and are calculated as follows: $X = (Z_{\max} + Z_{\min})/2$ and $M = (Z_{\max} - Z_{\min})/2$. The expressions for Airy beam $\overrightarrow{E}_{radm}$ and the exciting surface wave $\overrightarrow{J}_{surfm}$ are as follows:

$$\begin{cases} \overrightarrow{E}_{radmR} = \begin{pmatrix} \pm j\cos\theta_m\cos\varphi_m - \sin\varphi_m, \\ \pm j\cos\theta_m\sin\varphi_m + \cos\varphi_m, \\ +j\sin\theta_m \end{pmatrix} e^{-j\Psi_m} \\ \overrightarrow{J}_{surfm} = \frac{(x-x_m,y,z)}{r_{m(x,y)}} e^{-jk_{tm}\cdot t} = \frac{(x-x_m,y,z)}{\sqrt{(x-x_m)^2+y^2}} e^{-jk_{tm}\cdot t} \end{cases} \tag{2}$$

$(\pm j\cos\theta_m\cos\varphi_m - \sin\varphi_m, \pm j\cos\theta_m\sin\varphi_m + \cos\varphi_m, j\sin\theta_m)$ represents the CP beam in the direction of (θ_m, φ_m). $\overrightarrow{r}_{m(x,y)} = (x - x_m, y, 0)$ represents the coordinate vector from the excitation source at $(x_m, 0)$ to the (x, y) position of the THIMS. $\overrightarrow{k}_{tm} = (\sin\theta_m, 0, \cos\theta_m)$ is the transverse wave vector, and Ψ_m is the compensated phase to generate the mth circular Airy beam:

$$\begin{aligned} \Psi_m &= \arg\left\{Ai\left(b_{0(m)}\left(r_{0(m)} - r_{m(x,y)}\right)\right)\right\} \\ &\quad + l_m \arctan\left(\frac{y}{(x-x_m)}\right)\frac{2\pi}{\lambda}\overrightarrow{r}_{m(x,y)}\cdot\overrightarrow{u}_{0(m)} \end{aligned} \tag{3}$$

where $\overrightarrow{u}_{0m} = (\sin\theta_m\cos\varphi_m, \sin\theta_m\sin\varphi_m, \cos\theta_m)$ is related to the propagation direction of the mth beam. l_m, $Ai(\cdot)$, and $r_{0(m)}$ represent the OAM mode, Airy function, and the main ring radius in xoy plane at $z = 0$, respectively. The initial radius of the circular Airy beam is approximately equal to $(r_0 + 1/b_0)$. After a propagation distance z_f (autofocus distance) in the z direction, the maximum deviation for the Airy beam in the x direction is $D = b_0^3 z_f^2/4k^2$, where $k = 2\pi/\lambda$, λ is the wavelength, and b_0 is a constant, which can be obtained by setting the desired z_f and r_0. The radius shrinkage of the Airy beam from $(r_0 + 1/b_0)$ to 0 is equivalent to the deviation as follows [13]:

$$D = r_0 + 1/b_0 = b_0^3 z_f^2/4k^2 \tag{4}$$

Here, r_0 and z_f are assumed to be $0.1A$ (A is the aperture size of the THIMS) and 1080 mm, respectively, and from Eq. (4), $b_0 = 1.33r_0$.

From Eqs. (1)–(3), the surface impedance matrix components are obtained:

$$\begin{cases} Z_{xxm} = X_m + M_m\frac{x}{r_{m(x,y)}}\cos\theta_m \\ \qquad \cos\left(kx\sin\theta_m - k_{tm}\cdot r_{m(x,y)} + \Psi_m\right) \\ Z_{xym} = \frac{M_m}{2}\begin{pmatrix} \frac{y}{r_{m(x,y)}}\cos\theta_m\cos\left(kx\sin\theta_m\right. \\ \left. -k_{tm}\cdot r_{m(x,y)} + \Psi_m\right) \\ -\frac{x}{r_{m(x,y)}}\sin\left(kx\sin\theta_m\right. \\ \left. -k_{tm}\cdot r_{m(x,y)} + \Psi_m\right) \end{pmatrix} \\ Z_{yym} = X_m + M_m\frac{y}{r_{m(x,y)}} \\ \qquad \sin\left(kx\sin\theta_m - k_{tm}\cdot r_{m(x,y)} + \Psi_m\right) \end{cases} \tag{5}$$

where k_{tm} can be determined by:

$$k_{tm} = \sqrt{k_{xm}^2 + k_{ym}^2} = \sqrt{\phi_{xm}^2 + \phi_{ym}^2}/p \tag{6}$$

$$k = \frac{\omega}{c} = \frac{2\pi f}{c} \tag{7}$$

where Φ_x and Φ_y are the phase difference of the master-slave boundaries along x- and y-axes, respectively. p is the unit cell size. The tensor impedance calculation requires huge account operations, so in order to greatly simplify the design process of the unit cell, the effective scalar impedance $Z_e = k_z/k$ is used, which is the function of tensor impedance components and surface current direction θ_k as follows [11].

$$\begin{aligned} Z_e &= \frac{k_{zm}}{k_{0m}} = \left\{-j\left(\eta_0^2 - Z_{xym}^2 + Z_{xxm}Z_{yym}\right)\right. \\ &\quad \left. + \left[\begin{array}{l} -\left(\eta_0^2 - Z_{xym}^2 + Z_{xxm}Z_{yym}\right)^2 + 4\eta_0^2 \\ \times\left(Z_{yym}\cos^2\theta_{km} - Z_{xym}\sin 2\theta_{km}\right. \\ \left. +Z_{xxm}\sin^2\theta_{km}\right) \\ \times\left(Z_{xxm}\cos^2\theta_{km} + Z_{xym}\sin 2\theta_{km}\right. \\ \left. +Z_{yym}\sin^2\theta_{km}\right) \end{array}\right]^{1/2}\right\} \\ &\quad \times\left[2\eta_0\left(Z_{yym}\cos^2\theta_{km} - Z_{xym}\sin 2\theta_{km}\right.\right. \\ &\quad \left.\left. +Z_{xxm}\sin^2\theta_{km}\right)\right]^{-1} \end{aligned} \tag{8}$$

where η_0 is the impedance in free space. The relationship between k_z/k_0 and θ_k is an elliptic curve by Eq. (8). The major principal axis $Z_{e\max} = (k_z/k_0)_{\max}$ is the best impedance matching value, and the surface current direction would be dominated at the orientation of the principal axes angle $(\theta_{k\max})$.

3. UNIT CELL AND THIMS DESIGN

As an example, the millimeter-wave dual-frequency dual CP circular Airy OAM beams are generated: Beam-I: ($\theta_1 = 0$, $\varphi_1 = 0$, LHCP, $l = +1$, 36 GHz), Beam-II: ($\theta_2 = 0$, $\varphi_2 = 0$, RHCP, $l = 0$, 30 GHz). Two feeds J_{surf1} and J_{surf2} are at ($x_1 = 25$ mm, $y = 0$) and ($x_2 = -25$ mm, $y = 0$), respectively. All simulated results are derived from High Frequency Structure Simulator (HFSS). For the proposed structure, the average reactance $X_1 = 155\,\Omega$ and reactance modulation depth $M_1 = 60$ at 36 GHz, and $X_2 = 70\,\Omega$, $M_2 = 40$ at 30 GHz. $(\Phi_{x1}, \Phi_{y1}) = (0°, 90°)$ and $k_{t1} = 623.23$ at 30 GHz, $(\Phi_{x2}, \Phi_{y2}) = (0°, 110°)$ and $k_{t2} = 837.76$ at 36 GHz. The effective scalar impedance $(k_z/k)_{\max}$ at $(x, y, 0)$ is calculated by Eq. (8), and the $(k_z/k)_{\max}$ distribution in the THIMS is in Fig. 2. When it is excited by J_{surf1} solely, the impedance range is $52 \sim 105\,\Omega$ (Fig. 2(a)). When it is excited by J_{surf2}, the impedance range is $101 \sim 186\,\Omega$ (Fig. 2(b)). Then, the total tensor holographic impedance Z_{total} is obtained by the impedance superposition principle, which is shown in Fig. 2(c).

A tensor unit cell in Fig. 3 is proposed to implement the effective scalar impedance $(k_z/k)_{\max}$ distribution map in Fig. 2(c). The proposed unit cell consists of three layers of structure with a metal patch and a metal ground on each side of an F4B substrate

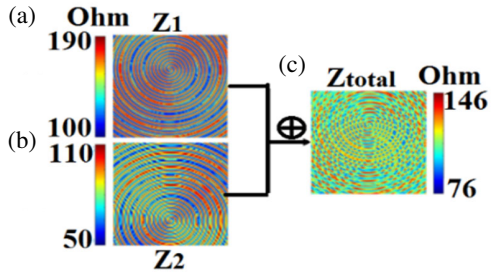

FIGURE 2. $(k_z/k)_{\max}$ distribution maps: (a) excited at port-1 solely; (b) excited at port-2 solely; (c) superposition results excited at dual ports.

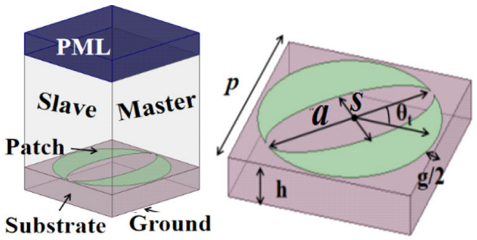

FIGURE 3. THIMS unit cell simulation structure.

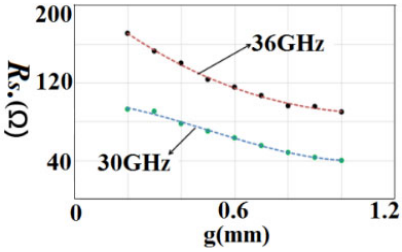

FIGURE 4. The relationship of $(g,\ Z_{e\max})$ at 30 GHz and 36 GHz.

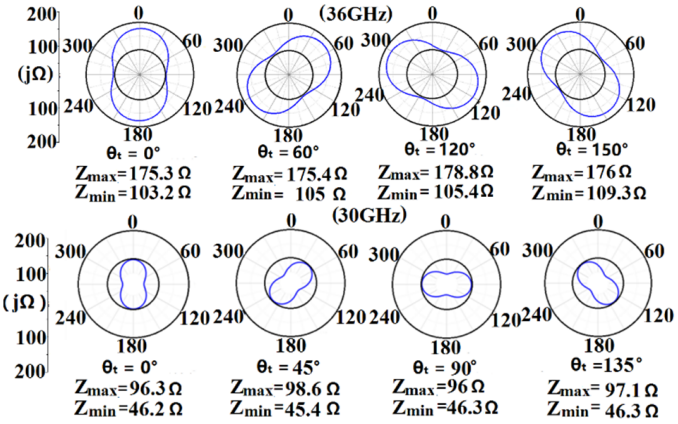

FIGURE 5. The relationship of $(g,\ Z_{e\max})$ at 30 GHz and 36 GHz.

(dielectric constant of 2.2 and thickness of 0.508 mm calculated according to [12]). The metal patch is a circular patch with an elliptical slot. The unit size $p = 2.5$ mm; the long axis a and short axis $s = 0.4 * a$ for the elliptical slot; the slot angle θ_t and the distance $g/2$ between the metal patch and edge are marked in Fig. 3. In order to simplify the design of the unit cell, Z_e is modulated by two degrees of freedom θ_t and g, and other geometry parameters are fixed. The slot angle θ_t is close to the major principal axis angle $(\theta_k)_{\max}$, and the slot angle θ_t has a small impact on $Z_{e\max} = (k_z/k_0)_{\max}$. $Z_{e\max}$ is mainly determined by geometry parameter g [11]. The simulated curves for $Z_{e\max}$ vs g are shown in Fig. 4 for 30 GHz and 36 GHz. When θ_t is 45°, and g is from 0.2 mm to 1 mm, the surface impedance (R_s) is in the range of $40 \sim 96\,\Omega$ and $106 \sim 177\,\Omega$ for 30 GHz and 36 GHz, respectively. The curves for $Z_{e\max}$ vs g for 30 GHz and 36 GHz are almost parallel, and the R_s at two frequency points can be controlled independently. After obtaining several discrete data sets of $(g, Z_{e\max})$, a polynomial formula for the relationship between $Z_{e\max}$ and g can be fitted as follows:

$$\begin{aligned} 30\,\text{GHz}\ \ g =& -4.0\times10^{-6}Z_{e\max}^3 + 8.8\times10^{-4}Z_{e\max}^2 \\ & - 0.1Z_{e\max} + 2.9 \\ 36\,\text{GHz}\ \ g =& -1.4\times10^{-6}Z_{e\max}^3 + 6.3\times10^{-4}Z_{e\max}^2 \\ & - 1.0Z_{e\max} + 6.0 \end{aligned} \tag{9}$$

According to Eq. (9) and Fig. 2, the geometry parameter g at position $(x, y, 0)$ is obtained. $\theta_t = (\theta_k)_{\max}$. Then the unit cells in the THIMS are decided.

The relationship between the slot angle θ_t and long axis direction $\theta_{k\max}$ is simulated for $g = 0.2$ mm. The curves for $Z_e = \alpha_z/k_0$ vs θ_k are simulated for $\theta_t = 0°, 45°, 90°, 135°$ at 30 GHz, and $\theta_t = 0°, 60°, 120°, 150°$ at 36 GHz. The results shown in Fig. 5 agree with the conclusion in [13]: The long axis angle $\theta_{k\max}$ is close to slot direction θ_t, that is $\theta_t = \theta_{k\max}$.

4. SIMULATED AND MEASURED RESULTS

Figure 6(a1) is the E-field distributions in yoz plane at $x = 25$ mm for Beam-I. The self-focusing occurs from $z = 625$ mm to 1200 mm for LHCP, and ND is up to 1.12 m, and long non-diffraction distance is obtained. Fig. 6(a2) is the E-field and phase distributions in xoy plane $z = 450$ mm, 1050 mm and 1200 mm. For the LHCP component at 36 GHz, the zero-intensity area in the plane center and the helical phase pattern indicate that the generated LHCP circular Airy OAM beam carries OAM mode $l = +1$. The cross polarization component (RHCP) is very little. Fig. 6(b1) is the E-field distributions in yoz plane at $x = -25$ mm for Beam-II. The self-focusing occurs from $z = 625$ mm to 1300 mm, and the diffraction-free distance is about 1.21 m. The E-field and phase distributions in xoy plane at $z = 450$ mm, 1050 mm, and 1200 mm are shown in Fig. 6(b2). There is no helical phase pattern and zero-intensity area in the plane center. The cross polarization component (LHCP) is very little. Therefore, at 30 GHz, the zero-order RHCP circular Airy OAM beam is generated. Fig. 7

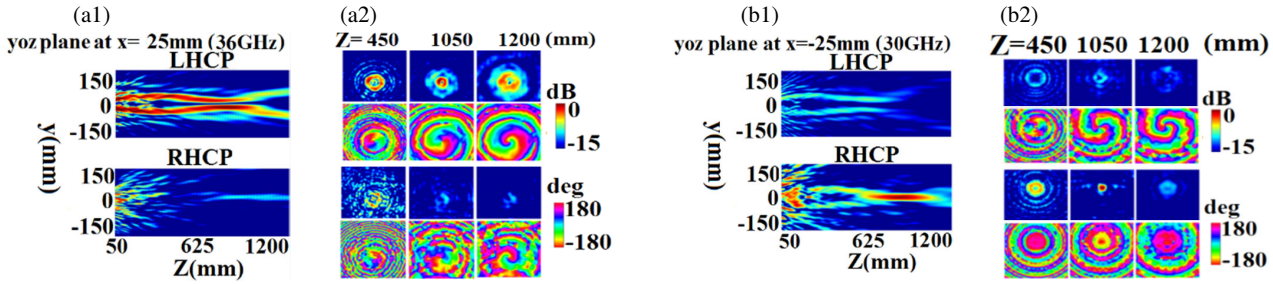

FIGURE 6. E-field distributions for LHCP and RHCP excited by port 1 and port 2 in yoz plane at $x = 25$ mm and xoy plane at $z = 450$ mm, 1050 mm and 1200 mm: (a) at 36 GHz; (b) at 30 GHz.

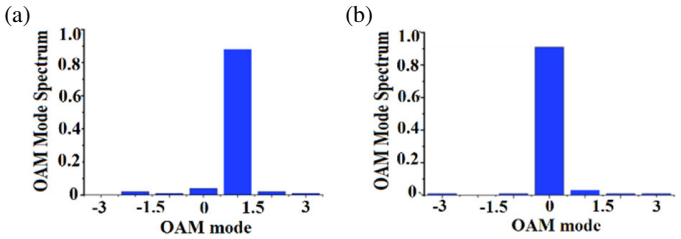

FIGURE 7. Simulated OAM spectrum weight of the sampled in $z = 1050$ mm plane: (a) LHCP at 36 GHz; (b) RHCP at 30 GHz.

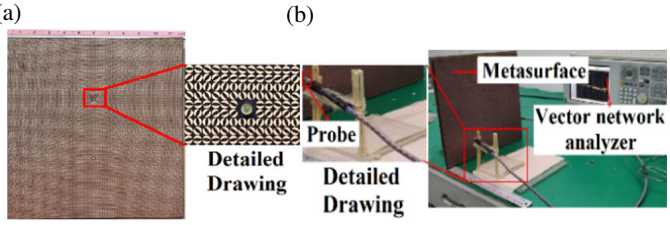

FIGURE 8. (a) The fabricated MS; (b) MS test environment.

TABLE 1. Comparisons with published Airy beam metasurface.

Ref.	f_0 (GHz)	Feeder	OAM mode	Aperture size $D(\lambda_0)$	$Z_{\mathrm{NDPD}}(\lambda_0)$	Z_{NDPD}/D	Polarization mode	Conversion efficiency (η)	OAM mode purity
[4]	1300	Horn	+1/+2/+3	—	4.35	—	Linear polarization	—	73%
[5]	10	Horn	—	11	—	—	LHCP	—	—
[14]	400	Horn	—	53.3	26.7	0.5	Linear polarization	90%	—
[15]	5.86	Horn	—	22	78	3.55	Linear polarization	—	—
[16]	47	Horn	+1	70.5	391.7	5.56	Linear polarization	—	—
Our work	Dual-frequency (30/36)	Monopole	0/+1	30/36	121/134.4	4.03/3.73	Dual-polarization (LHCP/RHCP)	42%/40%	89%/91%

shows that high OAM purities are obtained: 89% for Beam-I with $l = +1$ at 36 GHz, and 91% for $l = 0$ at 30 GHz.

Figure 8(a) is the prototype, and its near-field test environment is shown in Fig. 8(b). The test equipment is an Agilent N5230A-420 two-port network analyzer. Fig. 9 shows the simulated and measured electric field distributions in yoz plane at $x = 25$ mm/-25 mm for Beam-I and Beam-II at 36 GHz and 30 GHz. The simulated and measured results agree well. The measured maximum diffraction-free distances are 1.00 m for Beam-I and 1.05 m for Beam-II. The circular Airy beam CE (η) can be defined as the ratio of circular Airy OAM beam power $P_{1(2)}$ to the power (P_0) emitted by the feeder [17]. P_1 and P_2 are the power of Beam-I and Beam-II, respectively. The schematic for calculating the beam CE is in Fig. 10. The distance between the integral plane S with the size 150 mm $\times$ 150 mm and the THIMS is about 1050 mm. The calculated maximum beam CE is 42% at 30 GHz and 40% at 36 GHz.

Table 1 presents comparisons with published Airy beam metasurface antennas in feeder type, aperture size, -3 dB non-diffraction propagation distance (Z_{NDPD}), the radio of Z_{NDPD}/aperture size, polarization, and efficiency. Only our result is realized by THIMS, has low profile due to the feed from inside, and has the advantages of dual frequencies 30 GHz/36 GHz, long non-diffraction propagation distance $121\lambda_0/134.4\lambda_0$, high conversion efficiency 42%/40%, and high OAM purity 89%/91%. The THIMS can flexibly design highly efficient multifunctional dual frequency CP circular

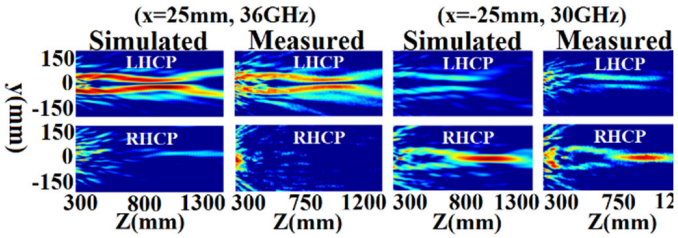

FIGURE 9. Simulated and measured electric field distributions at $f = 36$ GHz, 30 GHz in yoz plane.

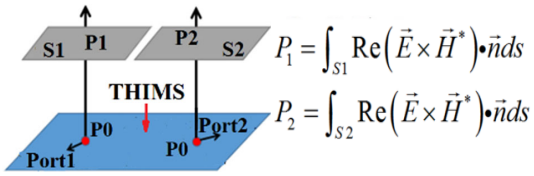

FIGURE 10. Schematic diagram of the beam conversion efficiency calculation method.

Airy beams with flexible co-modulation of OAM mode, polarization and beam direction.

5. CONCLUSION

In this paper, analytical formulas for THIMS are presented to generate CP circular Airy OAM multibeams with flexibly independent control of the individual beam direction, polarization, and OAM mode. As an example, a millimeter-wave THIMS is designed to generate dual frequency dual CP circular Airy OAM beams. The THIMS has the following advantages simultaneously: dual frequencies, dual CP, high CE (above 40%), long ND (up to $134.4\lambda_0$), high OAM purity (above 89%), co-modulation for polarization, beam direction, and OAM mode. The design method can be used to flexibly design other CP circular Airy OAM multibeams with independent control of OAM mode, direction, and polarization.

ACKNOWLEDGEMENT

This work was supported by the Guangdong Major Project of Basic and Applied Basic Research (2023B0303000008), the National Key Research and Development Program of China (2020YFB1807300), and the State Key Laboratory of Radio Frequency Heterogeneous Integration (Shenzhen University) No. 202306.

REFERENCES

[1] Efremidis, N. K. and D. N. Christodoulides, "Abruptly autofocusing waves," *Optics Letters*, Vol. 35, No. 23, 4045–4047, Dec. 2010.

[2] Mohanty, K., S. Mahajan, G. Pinton, M. Muller, and Y. Jing, "Observation of self-bending and focused ultrasound beams in the megahertz range," *IEEE Transactions on Ultrasonics, Ferroelectrics, and Frequency Control*, Vol. 65, No. 8, 1460–1467, Aug. 2018.

[3] Panagiotopoulos, P., D. G. Papazoglou, A. Couairon, and S. Tzortzakis, "Sharply autofocused ring-Airy beams transforming into non-linear intense light bullets," *Nature Communications*, Vol. 4, No. 1, 2622, Oct. 2013.

[4] Li, J.-S. and M. Zhong, "Airy beam multifunctional terahertz metasurface," *IEEE Photonics Technology Letters*, Vol. 35, No. 5, 245–248, Mar. 2023.

[5] Zhao, Z., X. Ding, K. Zhang, J. Fu, and Q. Wu, "2-D Airy beam generation and manipulation utilizing metasurface," *IEEE Transactions on Magnetics*, Vol. 58, No. 2, 1–5, Feb. 2022.

[6] Casaletti, M., M. Śmierzchalski, M. Ettorre, R. Sauleau, and N. Capet, "Polarized beams using scalar metasurfaces," *IEEE Transactions on Antennas and Propagation*, Vol. 64, No. 8, 3391–3400, Aug. 2016.

[7] Faenzi, M., G. Minatti, D. González-Ovejero, F. Caminita, E. Martini, C. D. Giovampaola, and S. Maci, "Metasurface antennas: New models, applications and realizations," *Scientific Reports*, Vol. 9, 10178, 2019.

[8] Ding, X., Z. Wang, G. Hu, J. Liu, K. Zhang, H. Li, B. Ratni, S. N. Burokur, Q. Wu, J. Tan, and C.-W. Qiu, "Metasurface holographic image projection based on mathematical properties of Fourier transform," *PhotoniX*, Vol. 1, 16, Jun. 2020.

[9] Meng, X., J. Wu, Z. Wu, T. Qu, and L. Yang, "Generating dual-polarization beams carrying dual orbital angular momentum modes based on anisotropic holographic metasurfaces," *Journal of Physics D: Applied Physics*, Vol. 52, No. 30, 305002, Nov. 2019.

[10] Emamian, H., H. Oraizi, and M. M. Moeini, "Design of wideband dual-beam leaky-wave antenna using the holographic theory," in *2019 27th Iranian Conference on Electrical Engineering (ICEE)*, 1456–1460, Yazd, Iran, 2019.

[11] Fong, B. H., J. S. Colburn, J. J. Ottusch, J. L. Visher, and D. F. Sievenpiper, "Scalar and tensor holographic artificial impedance surfaces," *IEEE Transactions on Antennas and Propagation*, Vol. 58, No. 10, 3212–3221, Oct. 2010.

[12] Faeghi, P., C. Ghobadi, J. Nourinia, and B. Virdee, "Nanoparticle-coated Vivaldi antenna array for gain enhancement," *Applied Physics A*, Vol. 129, No. 3, 217, Mar. 2023.

[13] Kadlimatti, R. and P. V. Parimi, "Millimeter-wave nondiffracting circular Airy OAM beams," *IEEE Transactions on Antennas and Propagation*, Vol. 67, No. 1, 260–269, Jan. 2019.

[14] Miao, Z.-W., Z.-C. Hao, B.-B. Jin, and Z. N. Chen, "Low-profile 2-D THz Airy beam generator using the phase-only reflective metasurface," *IEEE Transactions on Antennas and Propagation*, Vol. 68, No. 3, 1503–1513, Mar. 2020.

[15] Huang, Y., J. Li, H.-X. Xu, H. Yu, Z. Yang, P. Yu, W. Hu, D. Inserra, and G. Wen, "Experimental demonstration of microwave two-dimensional Airy beam generation based on single-layer metasurface," *IEEE Transactions on Antennas and Propagation*, Vol. 68, No. 11, 7507–7516, Nov. 2020.

[16] Huang, Y., X. Li, Z. Akram, H. Zhu, and Z. Qi, "Generation of millimeter-wave nondiffracting Airy OAM beam using a single-layer hexagonal lattice reflectarray," *IEEE Antennas and Wireless Propagation Letters*, Vol. 20, No. 6, 1093–1097, Jun. 2021.

[17] Yu, S., H. Liu, and L. Li, "Design of near-field focused metasurface for high-efficient wireless power transfer with multifocus characteristics," *IEEE Transactions on Industrial Electronics*, Vol. 66, No. 5, 3993–4002, 2018.